Rocket-Based Combined Cycle Flowpath Testing for Modes 1 and 4
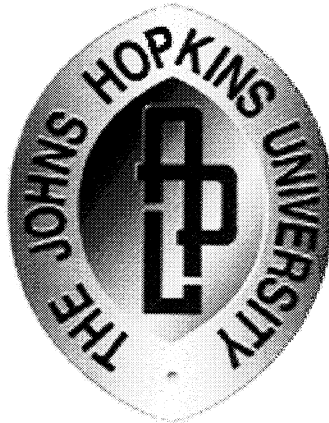
FINAL REPORT

Milton S. Eisenhower Research and Technology Development Center

October 15, 2002

THE JOHNS HOPKINS UNIVERSITY ◆ APPLIED PHYSICS LABORATORY
Johns Hopkins Road, Laurel, Maryland 20723-6099

Rocket-Based Combined Cycle Flowpath Testing for Modes 1 and 4

Submitted By:

Tharen Rice

Tharen Rice

Approved By:

D. M. VanWie

D. M. VanWie
Aeronautical Sciences and
Technology Group Supervisor

ABSTRACT

Under sponsorship of the NASA Glenn Research Center (NASA GRC), the Johns Hopkins University Applied Physics Laboratory (JHU/APL) designed and built a five-inch diameter, Rocket-Based Combined Cycle (RBCC) engine to investigate mode 1 and mode 4 engine performance as well as Mach 4 inlet performance. This engine was designed so that engine area and length ratios were similar to the NASA GRC GTX engine shown in Figure 1. Unlike the GTX semi-circular engine design, the APL engine is completely axisymmetric. For this design, a traditional rocket thruster was installed inside of the scramjet flowpath, along the engine centerline.

A three part test series was conducted to determine Mode 1 and Mode 4 engine performance. In part one, testing of the rocket thruster alone was accomplished and its performance determined (average I_{SP} efficiency = 90%). In part two, Mode 1 (air-augmented rocket) testing was conducted at a nominal chamber pressure-to-ambient pressure ratio of 100 with the engine inlet fully open. Results showed that there was neither a thrust increment nor decrement over rocket-only thrust during Mode 1 operation. In part three, Mode 4 testing was conducted with chamber pressure-to-ambient pressure ratios lower than desired (80 instead of 600) with the inlet fully closed. Results for this testing showed a performance decrease of 20% as compared to the rocket-only testing. It is felt that these results are directly related to the low-pressure ratio tested and not the engine design.

During this program, Mach 4 inlet testing was also conducted. For these tests, a moveable centerbody was tested to determine the maximum contraction ratio for the engine design. The experimental results agreed with CFD results conducted by NASA GRC, showing a maximum geometric contraction ratio of approximately 10.5.

This report details the hardware design, test setup, experimental results and data analysis associated with the aforementioned tests.

NOMENCLATURE

A	Area	A	Ambient conditions
C^*	Characteristic Exhaust Velocity	C	Chamber or Capture
F	Force, Thrust	e	Exit
I_{SP}	Specific Impulse	hub	Engine Hub Station
L	Length	vac	Vacuum
$\dot{m}$	Mass Flow	*	Throat
O/F	Oxidizer-to-Fuel Ratio	3	Rocket Exit Station
P	Pressure	6	Combustor Exit Station
V	Velocity		

Subscripts

BACKGROUND AND PROGRAM OBJECTIVES

Under grant NAG3-2333, the Johns Hopkins University Applied Physics Laboratory (JHU/APL) was initially funded by the NASA Glenn Research Center to conduct an analytical and experimental investigation of low-speed operation of a hydrocarbon-fueled Rocket-Based Combined Cycle (RBCC) engine [Ref. 1]. For a typical RBCC engine concept, from launch to approximately Mach 3, the engine runs in an air-augmented rocket (AAR) cycle (Mode 1). At Mach 3, the engine transitions from the AAR cycle to a ramjet/scramjet cycle (Modes 2/3). The engine transitions to an all rocket cycle (Mode 4) at approximately Mach 10. The operation of an HC-fueled RBCC engine cycle, especially below Mach 3 (AAR mode), had not been well documented or its performance sufficiently demonstrated; yet understanding AAR mode performance was and still is essential in the design of an RBCC engine. Without an accurate prediction of low-speed performance, engine sizing and therefore overall engine performance would be skewed. To begin to address the performance issues of an HC-fueled RBCC engine operating in AAR mode, the following four objectives were set forth.

1. Conduct an analytical investigation of a hydrocarbon (HC) fueled RBCC engine operating in air-augmented rocket mode.
2. Conduct an analysis of overall vehicle weight and size comparisons for an HC-fueled versus an LH_2- fueled air-augmented rocket system.
3. Conduct an analysis of optimal ramjet/scramjet takeover Mach number for system.
4. Conduct an experimental investigation of various engine parameters on air-augmentation effects of rocket thrust at Mach 0 and Mach 4 flight conditions for an HC-fueled system.

The experimental testing was to be conducted on an existing RBCC test rig designed and developed under APL internal funding. Early in the task (15% of the funding spent), a mutual agreement between the sponsor and APL was reached to modify the objectives as follows.

1. The existing test rig would be scrapped and a new test rig would be fabricated and tested. This new design would be a scaled axisymmetric version of the NASA GRC GTX engine [Ref. 2]. This design would be designated APL-10C.
2. Following with the GTX engine operation, hydrogen fuel would be tested instead of a hydrocarbon fuel.
3. Also, instead of looking at just AAR mode operation, an attempt would be made to test Mode 4 operation as well.
4. A new engine design would be developed to allow for a moveable engine centerbody so that Mach 4 inlet testing could be performed.
5. Perform four extensive test series, consisting of rocket-only, Mode 1, Mode 4 and Mach 4 inlet testing.

It was expected that these new objectives could be met without any funding increase; however, as will be discussed later, this was not the case, as objective 5 was not fully met.

4

EXPERIMENTAL TEST SETUP

Test Rig Overview

The APL-10C engine, shown in Figure 2, was designed to be a scaled, axisymmetric version of the GTX engine from the tip of the forebody to the end of the combustor. To accomplish this, GTX engine area ratios and length ratios were imposed on an axisymmetric skeleton to achieve the APL-10C design. Table 1 shows the pertinent engine ratios of both the baseline GTX and the APL-10C designs. All of the GTX engine ratios were successfully translated except for combustor area ratio (A_6/A_3). Matching this ratio would have created an unacceptable design where the combustor exit radius would have been greater than the cowl radius of 2.5 inches. This 2.5 inch limit was imposed because of facility starting issues that might have arisen during the Mach 4 inlet testing.

APL-10C was designed so that the engine centerbody could translate during a test. This feature was used extensively during the Mach 4 inlet tests. Two different mounting stings were designed and fabricated for these series of test. One sting was designed to connect to the aft end of the centerbody to allow for a clean centerbody during the inlet testing. A schematic of this design is shown in Figure 3. The other sting was used during the Mode 1 and Mode 4 tests. This design is shown in Figure 4.

All parts of the engine were designed to be heat-sink; no active cooling techniques were implemented in this design. The engine was mounted on a flexured thrust stand so that axial force measurements could be taken.

The rocket thruster, manufactured out of Nickel-200, was embedded in the aft end of the engine centerbody. The thruster had a throat radius of 0.21 inches and a nozzle expansion ratio of 5.0. At a chamber pressure of 500 psia, the rocket has the capability to produce approximately 100 lbf of thrust. Gaseous hydrogen was used as the fuel. Enriched air (50% O_2 by mole) was used as the oxidizer. These propellants were supplied to the thruster through a threaded Nickel-200 injector cap. This cap included single, perpendicular, like-doublet injectors for each propellant as well as a chamber pressure port and spark plug ignition housing. Figure 5 shows a schematic of the rocket thruster assembly. In previous testing, both the thruster assembly and injector cap were made out of 2% thoriated tungsten. In both cases, cracks appeared in the parts after several tests due to thermal cycling effects. This did not occur in the Nickel-200 parts.

Test Facility, Instrumentation and Control

The engine model was instrumented with 31 wall pressure taps, 7 on the centerbody and 24 on the cowl-side. Twenty-nine of the taps were along a common axial line. Two taps were located 180° from this common line. These measurements were taken at approximately 50 Hz. Figure 6 shows the locations of the pressure taps. Rocket thruster chamber pressure and gross thrust measurements were taken at approximately 100 Hz.

5

Fuel and oxidizer flow rates were controlled by varying the supply pressures upstream of sonic flow venturis. A schematic of the supply system is shown in Figure 7. Mass flow measurements were obtained by using the sonic throat method for a real gas. This method is explained in more detail in the data analysis section of this report.

All of the tests were conducted at the JHU/APL W. H. Avery Advanced Technology Development Laboratory (AATDL) Cell 2 Freejet Engine Facility (see Figure 8). Occupying five acres in the northeast area of the JHU/APL property, the AATDL is a stand-alone facility originally built to support ramjet engine development as well as internal and external aerodynamic studies. Over the past four decades, a diverse range of research and experiments have been performed that have expanded the capabilities of the AATDL to encompass many areas that are applicable to combined-cycle engine technology hurdles. They include basic research on fuel penetration and mixing, shock-wave/boundary-layer interactions, component testing of inlet, combustors (H_2 and HC- fueled) and nozzles, freejet testing of complete scramjet and RBCC engines, and research in plasma-aerodynamics for a wide range of applications including drag reduction and advanced ignition techniques.

The test cells at the Avery Laboratory are blowdown to vacuum in nature. Up to 775,000 Standard Cubic Feet (SCF) of air is stored at pressures up to 3000 psia. Flow rates up to 150 lbm/s are possible. High velocities are produced by heating the air prior to passing through one of five test cells. Both storage and combustion heaters are used allowing simulation of conditions up to Mach 8 flight velocities. The facility maintains both hydrogen and oxygen supply systems that are used for the combustion heaters. A steam exhaust system is available that provides altitude simulation up to approximately 110,000 feet. Three different cooling water supply systems are available: 1100 GPM at 90 psia, 500 GPM at 250 psia, and 1500 GPM at 2000 psia. An 11,450 SCF, 3000-psia hydrogen fuel supply system is available capable of delivering hydrogen to the test cells at flow rates up to 1.1 lbm/s. Numerous other small-scale gas systems are available throughout the facility for supply of nitrogen, argon, helium, etc.

RESULTS & DISCUSSION

Rocket-Only Testing

The rocket thruster was tested by itself to baseline performance for the later Mode 1 and Mode 4 tests. Figure 9 shows the rocket thruster during a test in the Cell 2 test facility. For this test series, gross thrusts at various O/F ratios and a nominal 500 psia chamber pressure were obtained. As stated previously, the rocket thruster uses enriched air as the oxidizer and hydrogen as the fuel. The primary reason for choosing enriched air over pure oxygen was to reduce the thermal loads in the thruster by reducing the total temperature. Looking ahead to the Mode 1 testing, where the amount of the unreacted hydrogen may be critical to engine performance, careful attention was paid to keeping the equivalence ratio (1.32) consistent between the APL-10C thruster and a GTX rocket thruster (O_2/H_2) operating at an O/F = 6. To meet that criteria, the nominal O/F ratio for the APL-10C thruster was set to 11.23.

Nominal supply and chamber pressure data is shown in Figure 10. Nominal thrust data is shown in Figure 11. For both sets of data, average values were calculated over the steady-state

portion of the data trace, as noted in the figures. Thrust data was obtained by averaging the data during the rocket firing and correcting that value with an averaged tare value as shown in Figure 11. Fuel and oxidizer mass flow was calculated using the sonic throat method for a real gas, as follows.

$$\dot{m} = P_T A^* \left[\frac{P/P_T}{\sqrt{T_T}} \overset{\circ}{m} \right]^*$$ (1)

$$P/P_T = \left(1 + \frac{\gamma-1}{2} M^2 \right)^{\gamma/\gamma-1}$$ (2)

$$\overset{\circ}{m} = \sqrt{\frac{g\gamma}{R}} M \left(1 + \frac{\gamma-1}{2} M^2 \right)^{1/2}$$ (3)

Where P_T and T_T are the pressure and temperature upstream of the venturi respectively. M = 1.0, R = 51.490 lbf-ft/lbm-°R for enriched air and R = 766.4 lbf-ft/lbm-°R for hydrogen. Figure 12 shows a schematic of the mass flow venturi.

When implementing a real gas calculation, the γ of the enriched air changes as a function of pressure, and to a slight degree temperature. Using the FLUID real gas properties code, a data table of γ versus pressure was created for both nitrogen and oxygen. These values were then averaged. A linear fit of the data was created and then used to determine γ for a given venturi pressure. Figure 13 shows a plot of the three sets of data. The same analysis was conducted as a function of temperature. The resulting γ remained nearly constant over the range of temperatures (512-540 °R) seen during testing, so it was not included in the analysis. As a note a constant γ of 1.4 was used for hydrogen.

From the data, a nominal gross I_{SP} and I_{SP} efficiency of 267 sec, and 90.3% respectively were obtained. Gross thrust is a taken directly from the load cell measurement data. Gross thrust and I_{SP} are defined as follows:

$$F_{gross} = \dot{m} V_e + A_e (P_e - P_a)$$ (4)

$$I_{SP} = \frac{F_{gross}}{\dot{m}}$$ (5)

I_{SP} efficiency for each run was also calculated. I_{SP} efficiency is defined as the experimental I_{SP} divided by the ideal 1-D equilibrium I_{SP} when isentropically expanded to the ambient pressure, assuming a nozzle efficiency of 100%.

$$I_{SP} Efficiency = \frac{[I_{SP}]_{measured}}{[I_{SP}]_{1-D,equ,P_{exit}=P_a}}$$ (6)

7

Table 2 shows a summary of the rocket-only test data as well as summaries for the Mode 1 and Mode 4 testing that is detailed later in this report. Also shown in Table 2 is the characteristic exhaust velocity, C*, which is defined as follows.

$$C^* = \frac{P_c A^*}{\dot{m}} \tag{7}$$

At this point, some discussion on the design evolution of the rocket thruster should be done. In FY99, APL undertook an internal research and development (IRAD) effort to investigate Mode 1 performance of a high L/D, RBCC engine for tactical missile applications. Figure 14 shows a schematic of the engine flowpath. For this effort a rocket thruster was designed and built. Testing of the thruster-only as well as the engine in Mode 1 was conducted. The results are discussed in Reference 3. The data from the thruster-only tests showed and average I$_{SP}$ efficiency of 75%. A thermal analysis that was conducted on the thruster design showed that up to 10% of the total loss could be caused by heat loss. The remaining 20% was attributed to the simple injector design as well as the short combustion chamber length.

As the current APL-10C thruster was being designed, attention was paid to the previous flaws so that they would not be repeated. Figure 15 shows a comparison of the two designs. Note that the injector design was changed from a simple unlike-doublet design to a perpendicular, like-doublet design. Also note that combustion chamber was lengthened by 60%. Figure 16 shows a comparison of thruster performance. As seen, a performance increase of approximately 20% was realized. Applying the heat loss performance decrement of 10% from the previous thermal analysis to the current design showed that the current thruster could be operating at nearly 100% efficiency if the heat loss were recouped, as would be the case in an regeneratively cooled design. No attempts of this nature were implemented however.

Mode 1 Testing

During Mode 1 operation of an RBCC engine, two different engine cycles have been hypothesized. The most commonly assumed hypothesis is the ejector-ramjet cycle where air entrained through the inlet system increases engine performance as it mixes and burns with the fuel-rich affluent of the rocket exhaust. The other hypothesis, used in the GTX engine cycle analysis, is the Independent Ramjet Stream (IRS) Cycle, where the airstream does not mix with the rocket exhaust and is fueled and combusted independently. This in theory would decrease the required duct length to mix and burn the two streams [Ref. 4]. The APL-10C engine was not equipped with independent airstream fuel injectors, so the IRS cycle could not be tested; however, a series of static tests were conducted on the APL-10C engine to test its effectiveness operating in the ejector-ramjet cycle. Figure 17 shows the entire engine installed in the JHU/APL Cell 2 facility. Figure 4 shows a schematic of the as tested engine.

During Mode 1 operation, GTX operates its rocket thrusters at a 2000 psia chamber pressure and an O/F ratio of 6. Note that the inlet is positioned fully open to allow for maximum air entrainment. The APL-10C rocket thruster operates with a chamber pressure of 500 psia. To simulate the GTX thruster with a chamber pressure of 2000 psia operating at sea-level static

conditions, a nominal ambient pressure of 3.7 psia was needed to match the GTX chamber pressure-to-ambient pressure, $P_c/P_a = 136$. Ambient pressure was controlled through the use of the AATDL's steam ejector system that exhausts the test cabin down to the correct pressure during a test.

Due to limited funding and difficulties in igniting the rocket engine at sub-atmospheric pressures, only two Mode 1 tests were conducted. A nominal pressure ratio of 100 was achieved, resulting in a gross I_{sp} efficiency equal to that of the rocket-only testing. Gross I_{sp} efficiency as wells as C^* were calculated the same way as the rocket-only tests [Eqs. 6,7]. This means that there was neither an increase nor decrease in engine thrust due to air entrainment for this series of tests. Table 2 shows a summary of the test results. Figure 18 shows a plotted comparison of the Mode 1 and rocket-only performance data. Appendix B shows the complete data analysis methodology for all test series.

A plot of engine pressures versus time is shown in Figure 19. All of the engine pressures fall as the test cabin is being evacuated. When the rocket engine is ignited, the engine pressure vary, but by less than 1 psi. Figure 20 shows an average of the engine pressures as a function of their axial location. Again, the pressures vary only to a small degree meaning that airflow through the engine is minimal. These results run contrary to CFD results generated by NASA GRC that shows a near-sonic condition of the inlet airstream is achieved downstream of the rocket exit plane[Reference 4]. Figure 21 shows a Mach number plot of the CFD data. This discrepancy cannot be resolved with the limited data available. One possible reason for the differences is the way the Mode 1 test was run. To match ambient pressure the entire engine was placed in an enclosed test cabin attached to an ejector system. Only the air in the test cabin was available to be entrained in the inlet. This arrangement may have prevented air from being entrained. The CFD analysis on the other hand was conducted with an unlimited air supply.

Mode 4 Testing

For a nominal RBCC vehicle trajectory, Mode 4 begins at approximately Mach 10, at altitudes exceeding 90,000 feet. For this series of tests the APL-10C engine was tested, expect now the inlet was fully closed as shown in Figure 22. When attempting to test at this near-vacuum condition, special attention was paid trying to match the overall thruster pressure ratio. Testing at pressure ratios lower than required, might result in flowfield differences that would affect overall engine performance. For example, a lower than desired pressure ratio may prevent the rocket thruster plume from filling the entire engine cavity and/or may cause separated nozzle flow due to the flow being overexpanded.

Testing the full GTX engine with an overall rocket-throat-to-nozzle-exit area ratio exceeding 400 would require P_c/P_a ratios in excess of 10,000. This pressure requirement is lowered for the APL-10C testing due to the fact that the engine was only built to the end of the combustor, lowering the engine area ratio. Assuming an isentropic expansion from the rocket throat to the combustor exit of the APL-10C engine ($A_6/A^* = 147$), a pressure ratio, P_c/P_6 of 3200 was needed.

Even though the Cell 2 facility has the capability to test at low ambient pressures (< 1 psia) during freejet testing, it is limited to approximately 3 psi when testing in a static mode (no flow) as was done for the Mode 4 testing. This combined with the aforementioned difficulties in igniting the rocket engine at low ambient pressure yielded a maximum test pressure ratio of 82. Due to this, the results from these tests are not of great benefit in determining the overall Mode 4 engine performance. Table 2 shows a summary of the results. As is shown, these tests resulted in a nominal 10% decrease in performance of the rocket engine by itself. Figure 18 shows a plot of performance for various Mode 4 pressure ratios. As can be seen, as the pressure ratio increases, so does performance. It can only be presumed that this trend will continue to where Mode 4 performance will exceed rocket-only performance at near-vacuum pressure ratios.

Mach 4 Inlet Testing

The main objective of this test series was to determine the maximum experimental inlet contraction ratio of the APL-10C engine at Mach 4. To accomplish this, the APL-10C forebody and inlet cowl were installed in Cell 2 as shown in Figure 23. As is shown, a rear mounted sting was used to provide a clean centerbody flowfield for the tests. In an attempt to match the cowl lip Reynolds number of the full scale GTX vehicle, cold air was used as the test gas. Table 3 shows a comparison of pertinent testing parameters for a nominal Mach 4 GTX trajectory point and the as tested APL-10C engine. Note that the difference in Reynolds number led to a difference in the approximated values of a turbulent boundary layer at the cowl station. This difference however, did not seem to greatly affect the results.

At the start of each test, the inlet was positioned to its fully open position to allow it to start. Figure 24 shows a shadowgraph of the started inlet. Note the shocks that appear due to the leading edge of the forebody as well as the shock created by ramp surface external to the cowl lip. After the inlet was started, the centerbody was translated rearward until unstart occurred. Figure 25 shows a shadowgraph of the unstarted flowfield, where very little shock structure is present. The inlet was then translated forward to restart the inlet and reset to its initial position. Figure 26 shows a shadowgraph of the inlet just before the inlet restarts. The separation region shown in front of the inlet was immediately swallowed after this picture was taken as the inlet continues to open. To save testing time, the inlet was translated twice during one run of the tunnel.

Figure 27 shows a plot of the wall pressures just upstream of the nominal throat during two inlet translations. The peak pressures noted in the plot represent where the inlet unstarted. Inlet position was determined through the use of a calibrated string-pot device. One end of this device was attached to the moveable inlet centerbody and the other was connected to the fixed thrust stand. The entire inlet centerbody and sting mechanism was connected to a remotely controlled motion system. As the centerbody was translated, the string-pot device output a varying voltage reading that was then converted into distance using the device calibration. The string-pot output is also shown in Figure 27. With this, plus the inlet starting point (measured directly off of the rig), the unstart position could be determined. Contraction ratio was determined by calculating the difference in cowl side and centerbody radii at the inlet unstart position. Radii were taken directly from the as-built CAD drawings of the engine.

10

Table 4 shows a summary of the results for the five inlet sweeps tested. An average maximum contraction ratio of 10.32 was obtained. The resultant air capture ratio based on inlet positions and a conical flowfield is also shown in Table 4. Concurrent to the inlet testing, NASA GRC analyzed the GTX inlet using CFD for a similar Mach 4 condition [Ref. 5]. Figure 28 shows a comparison of the experimental and some of the CFD results. In the figure, pressure ratio as a function of centerbody position is plotted for a contraction ratio of 9.2. Note, at X/Rc = 0.0, the cowl and body-side steps are aligned. Other CFD showed an unstarted solution at 12.0, which is consistent with experimental results. The maximum pressure obtained in the CFD results was not obtained from the experiments because the pressure tap near the centerbody throat (x = -2.1 in Figure 28) was leaking to the atmosphere during testing.

SUMMARY

An axisymmetric version of the GTX engine was successfully designed, built and tested at APL. The engine, designated APL-10C, matches the GTX engine area and length ratios up to the combustor exit plane. Four different test series were conducted with this model as follows. Rocket-only testing was conducted to determine baseline performance. Mode 1 testing was conducted with the rocket embedded in the engine flowpath and the inlet system fully open. Results showed that there was neither a thrust increment nor decrement over the rocket-only testing. Mode 4 testing was conducted with the inlet fully closed. Lower than desired chamber-to-ambient pressure ratios were tested resulting in a 20% lower Mode 4 performance over the baseline rocket-only testing. This was determined to be function of the pressure ratios tested and is likely not due to the engine design. The final test series consisted of testing the engine's inlet system at Mach 4 flight conditions. The results from these tests were consistent with results from NASA GRC generated CFD.

The rescoping of efforts early in the program was the primary reason for the deficiency in the amount of quality data generated. The original program scope included hydrocarbon testing of an already existing engine design. The rescoped program included the design and fabrication on an entirely new and more complicated engine. Initially it was thought that this could be accomplished while remaining at the current funding level. This proved to be an optimistic view as several technical challenges (mainly rocket ignition in sub-atmospheric pressures and achieving higher than desired pressure ratios) arose. The funding needed to tackle these challenges ultimately led to a significantly smaller test series than desired.

REFERENCES

1. Rice, T., "Rocket-Based Combined Cycle Flowpath Testing for Modes 1 and 4," Unsolicited Proposal to NASA GRC, AD-20830, October, 2000.

2. Trefny, C. J., "An Air-Breathing Launch Vehicle Concept for Single-Stage-to-Orbit," AIAA-99-2730, Presented at the 35th AIAA/ASME/SAE/ASEE Joint Propulsion Conference, Los Angeles, CA, June 1999.

3. Rice, T., "Static Thrust Augmentation Due to Air-Entrainment of a Hydrogen-Fueled RBCC Engine," Presented at the 2000 JANNAF CS/APS/PSHS/MSS Joint Meeting, Monterey, CA, November 2000.

4. Steffen, C. J., Jr. and Yungster, S., "Computational Analysis of the Combustion Processes in an Axisymmetric, RBCC Flowpath," Presented at the 2000 JANNAF CS/APS/PSHS/MSS Joint Meeting, Monterey, CA, November 2000.

5. DeBonis, J. R., Steffen, C. J. Jr., Rice, T., and Trefny, C. J., "Design Evolution and Performance Characterization of the GTX Air-Breathing Launch Vehicle Inlet," Presented at the 2002 JANNAF CS/APS/PSHS/MSS Joint Meeting, Destin, FL, April 2002.

TABLES AND FIGURES

Table 1. GTX and APL-10C Engine Ratios

| | | GTX 10c | | APL-10C | |
| | | in | sq.in. | in | sq.in. |
Station	Detail	Radius	Area	Radius	Area
C	Total Capture Area		6634	2.5	19.635
*	Rocket Throat	3.794	45.22	0.2064	0.134
exit	Rocket Exit	8.483	226.1	0.4615	0.669
3	Combustor entrance		2654	1.581	7.853
6	Combustor exit		8292	2.500	19.635
hub	Hub exit		503.7	0.689	1.491
	Ac/A3		2.500		2.500
	Aexit/A*		5.00		5.00
	A6/A3		3.125		2.500
	A3/A*		58.68		58.68
	Ahub/A3		0.1898		0.1898
	L6-3/DH3		3.234		3.234

Figure 1. GTX Vehicle Concept

Figure 2. APL-10C RBCC Engine
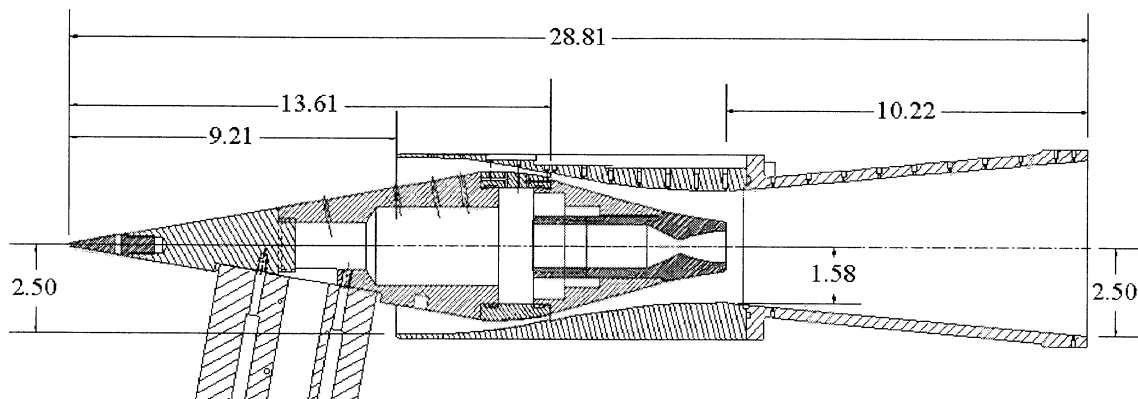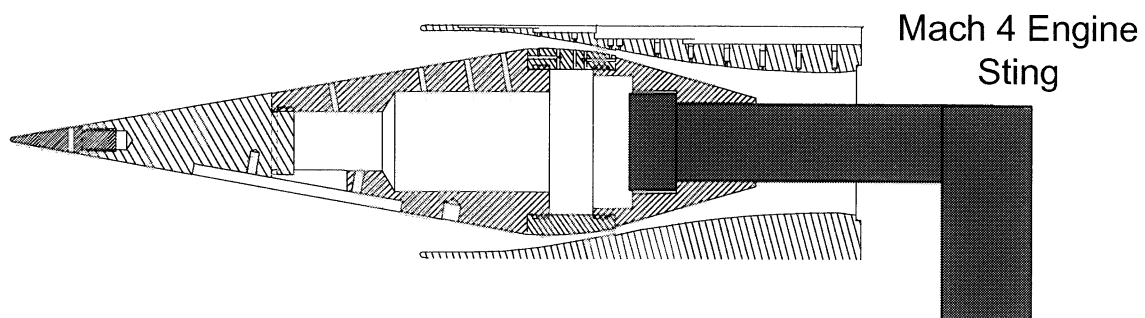

Mach 4 Engine
Sting

Figure 3. APL-10C Engine with Mach 4 Inlet Testing Sting
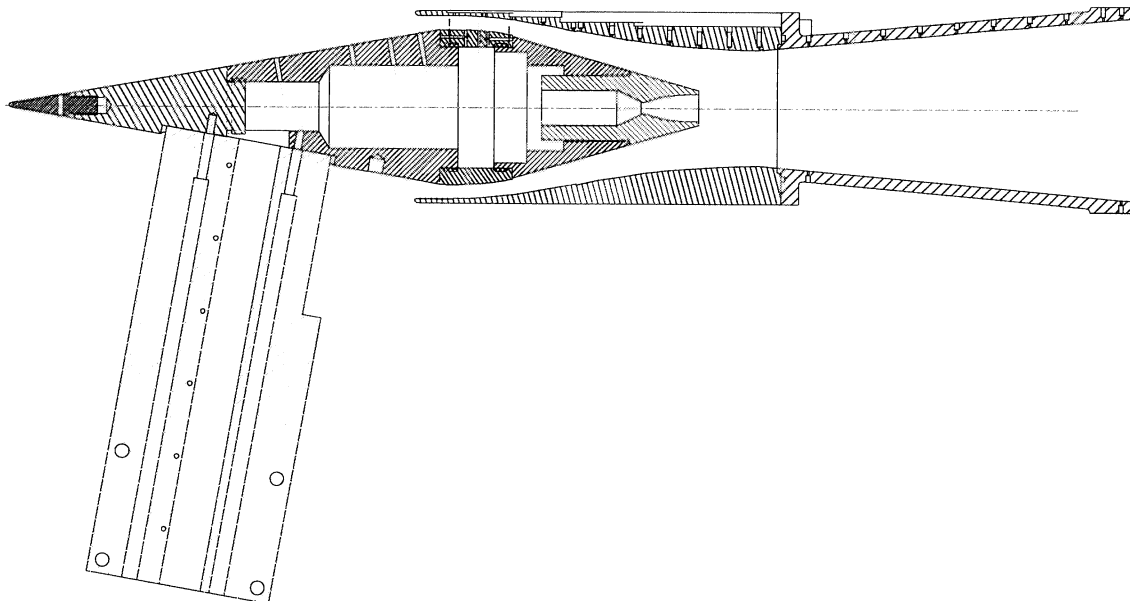
Figure 4. APL-10C Engine with Modes 1 & 4 Sting
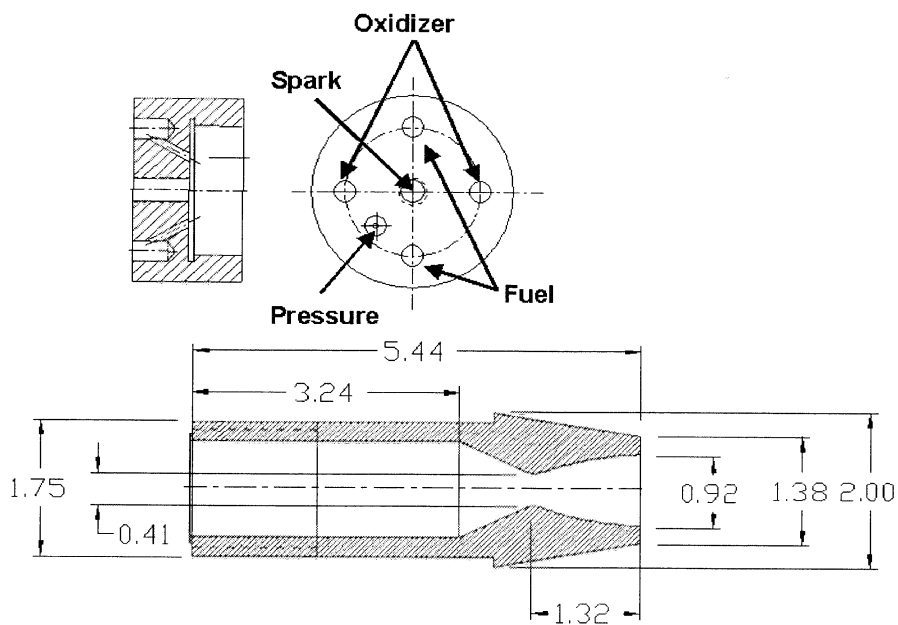

Figure 5. Rocket Thruster Assembly for APL-10C Engine
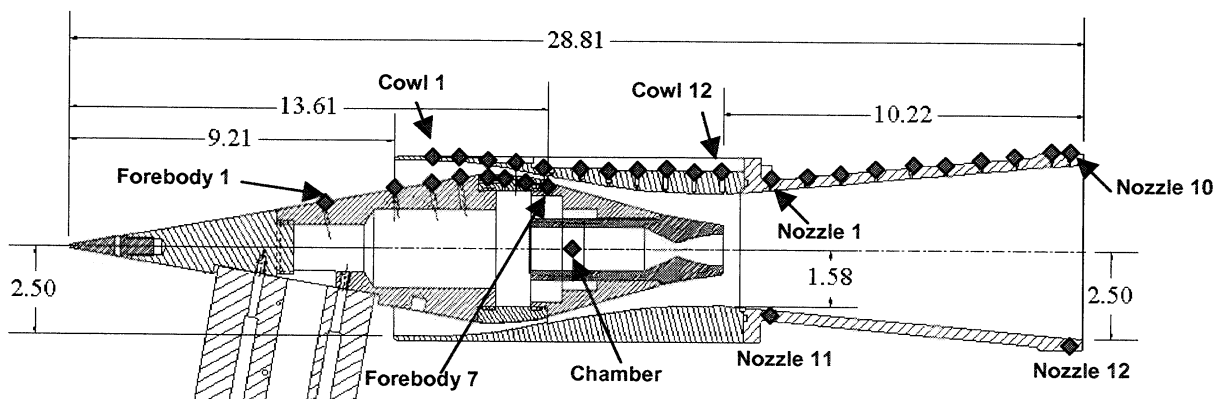
Figure 6. Pressure Tap Locations
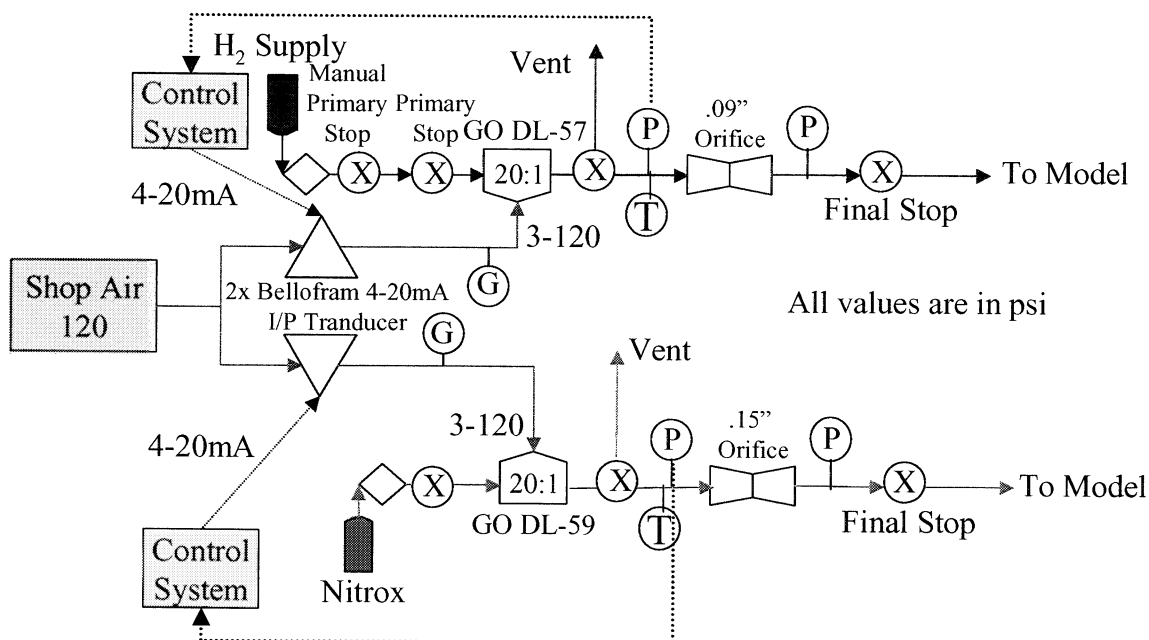
Figure 7. Fuel and Oxidizer Supply Control System
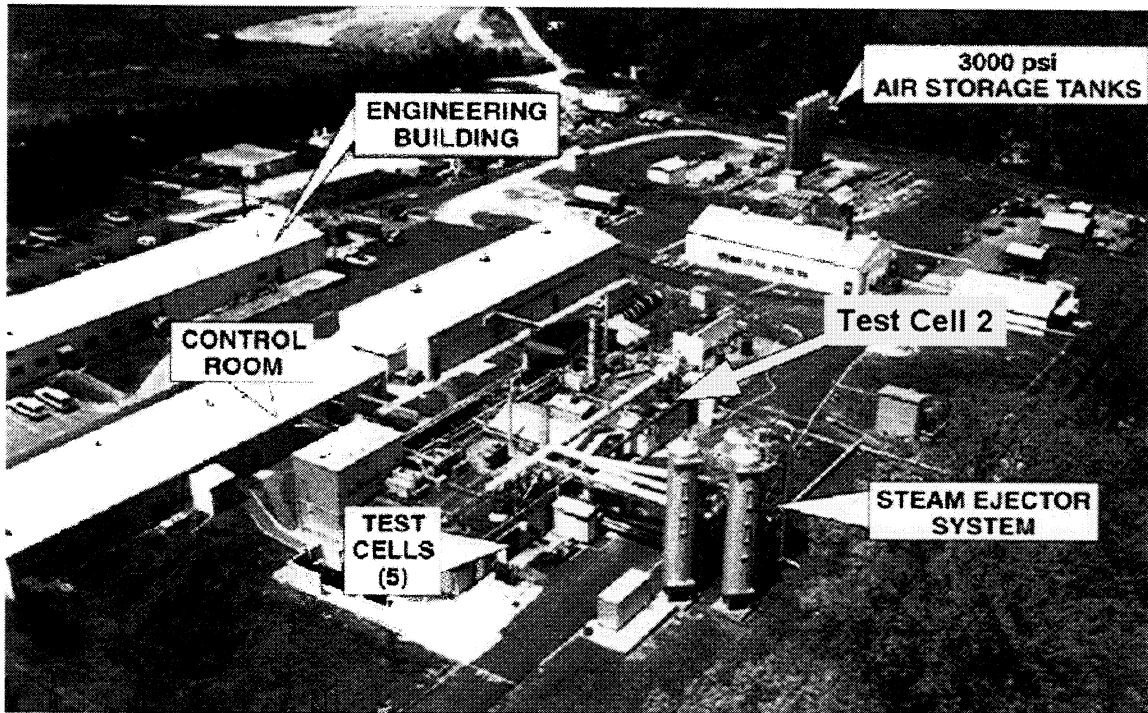
Figure 8. The JHU/APL Avery Advanced Research and Technology Development Laboratory
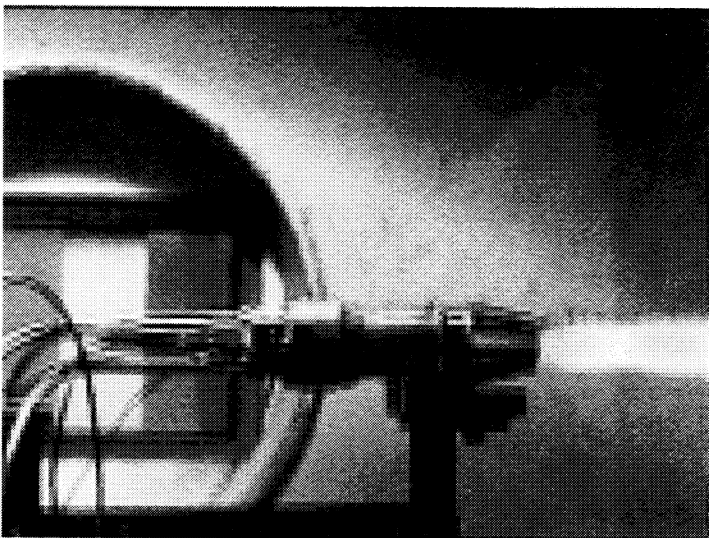
Figure 9. APL-10C Rocket Thruster During Testing

17
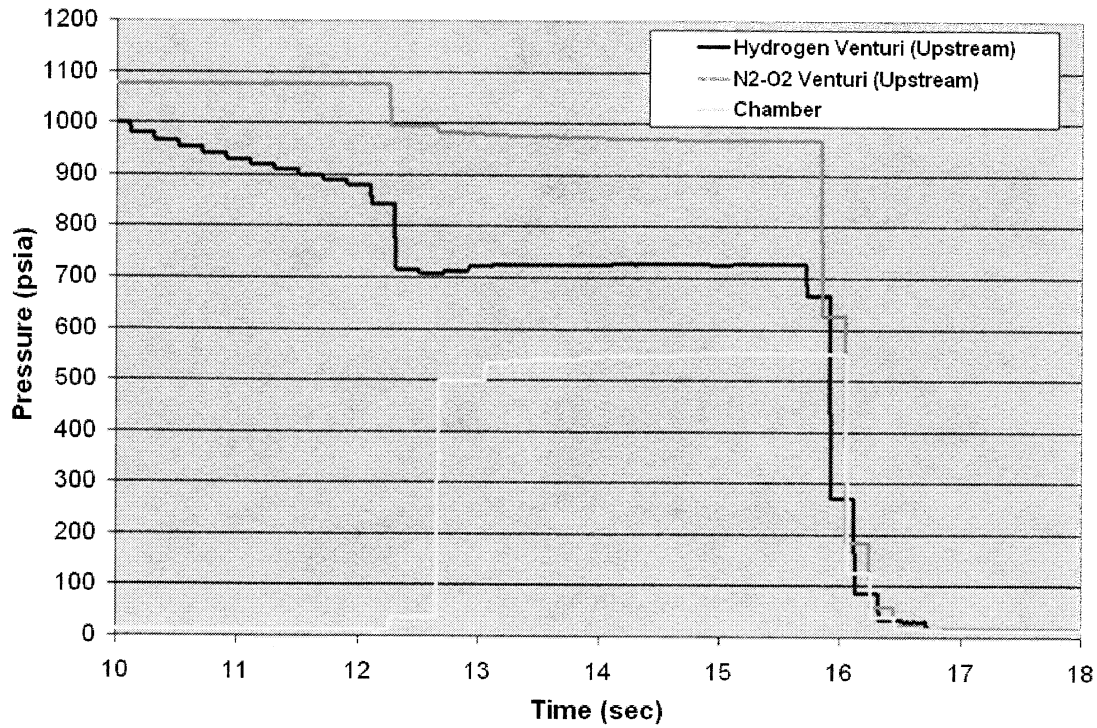
Figure 10. Nominal Supply and Chamber Pressure Data
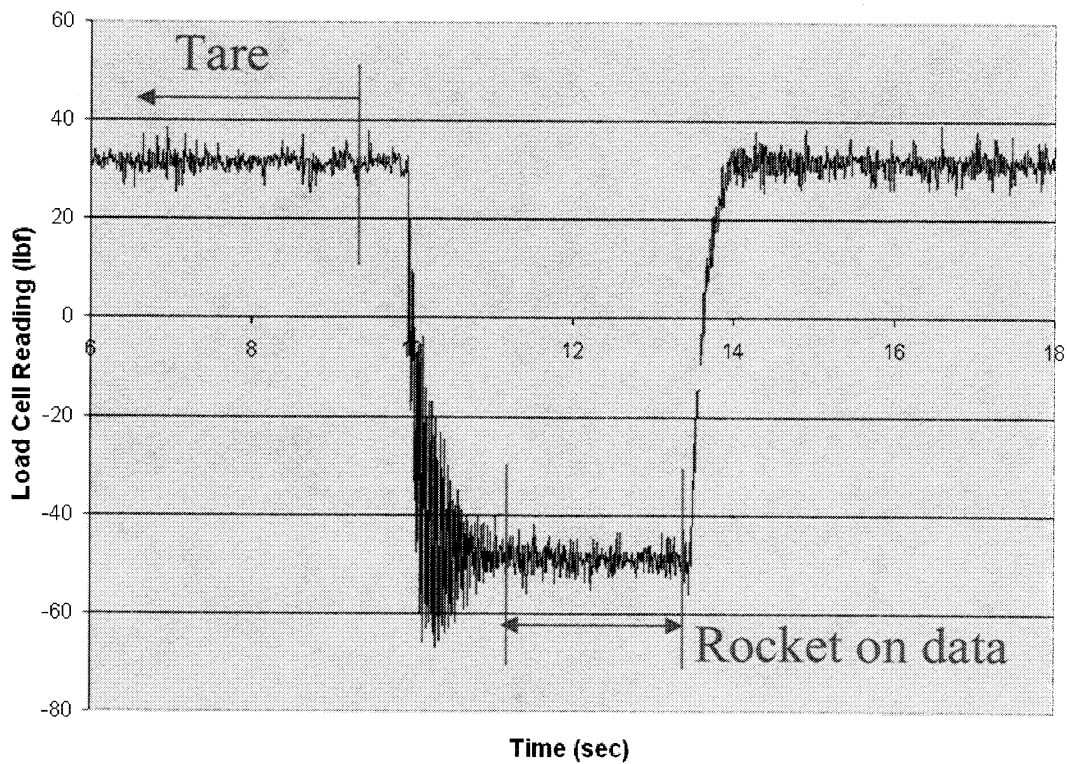
Figure 11. Nominal Thrust Data

18
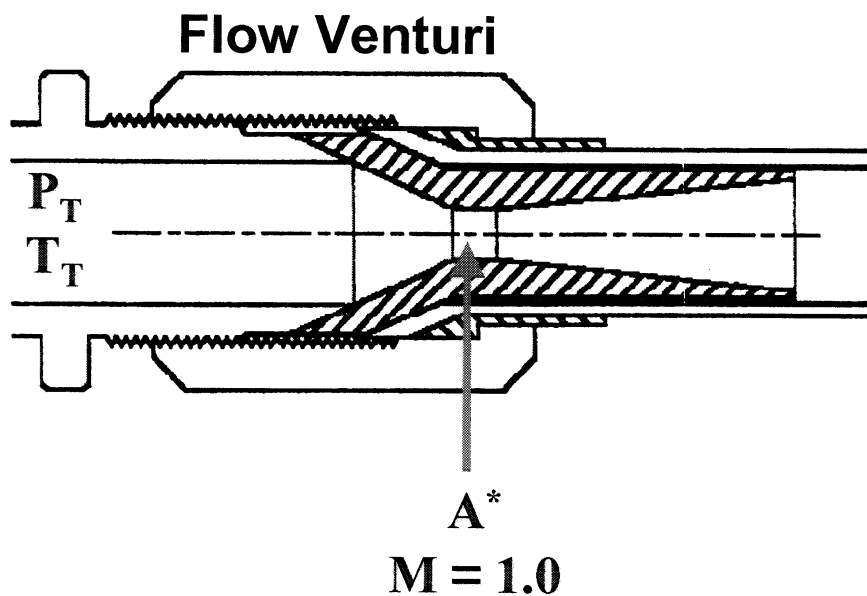
Flow Venturi

Figure 12. Venturi Mass Flow Calculation Schematic
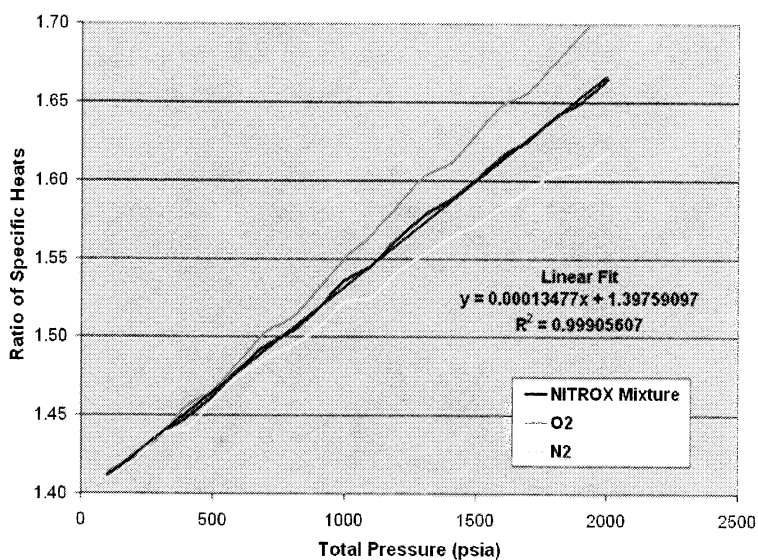
Figure 13. Oxidizer Gamma Variation Versus Pressure

Figure 14. Flowpath of APL IRAD RBCC Engine

APL-10C Rocket Thruster   **IR&D Rocket Thruster**
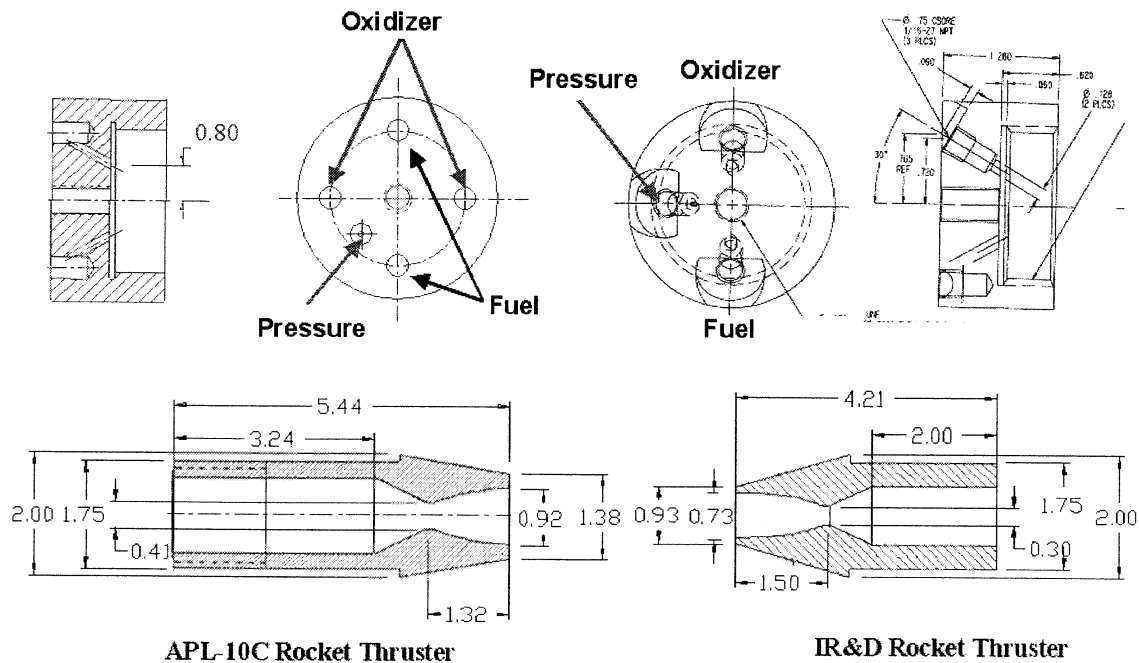
Figure 15. Comparison the APL-10C Thruster and the Previous IRAD Thruster

$$Gross\ I_{SP}\ Efficiency = \frac{Measured\ I_{SP}}{[I_{SP}]_{1-D, P_{exit}=P_a}}$$
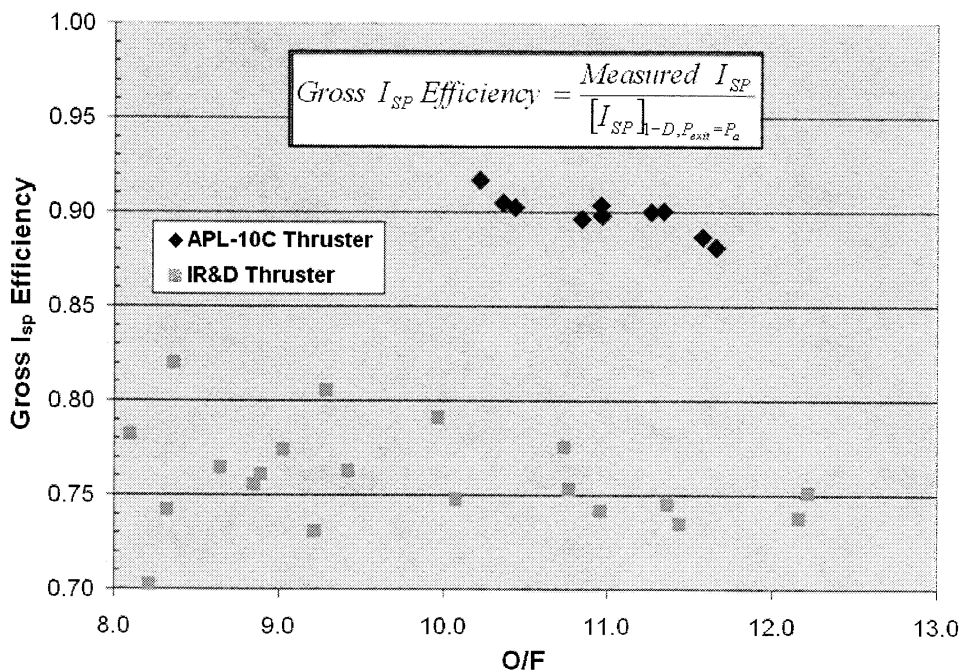
Figure 16. Thruster Performance Comparison
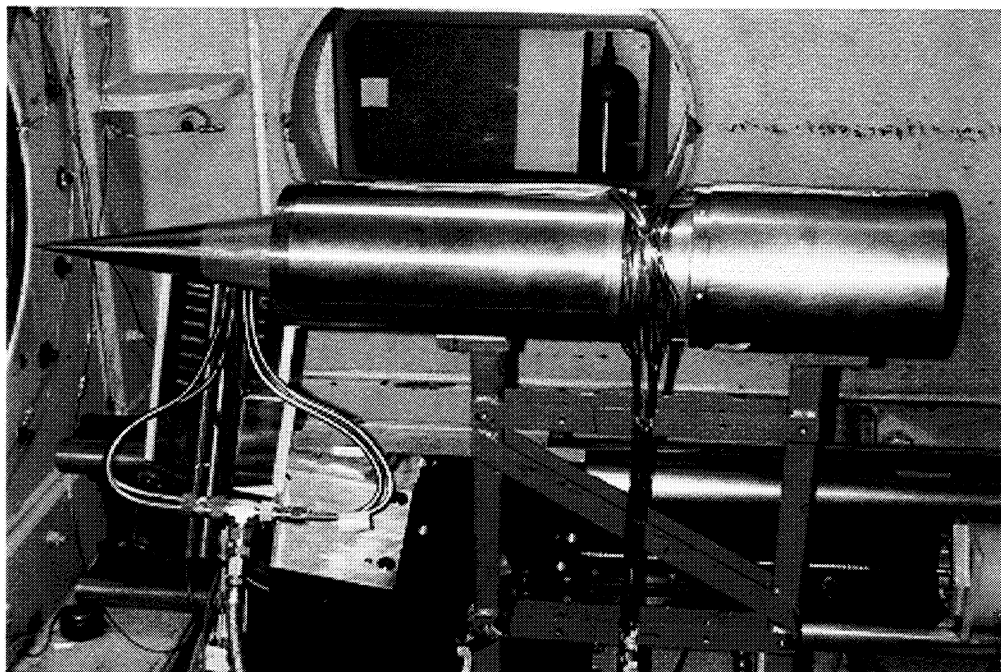
Figure 17. Modes 1 & 4 Engine Installation in the Cell 2 Freejet Engine Facility

$$Gross\ I_{SP}\ Efficiency = \frac{Measured\ I_{SP}}{[I_{SP}]_{1-D,P_{exit}=P_a}}$$

Legend:
- ◆ Rocket-Only
- Mode 4: Pc/Pa = 35
- Mode 4: Pc/Pa = 80
- Mode 1: Pc/Pa = 90-115
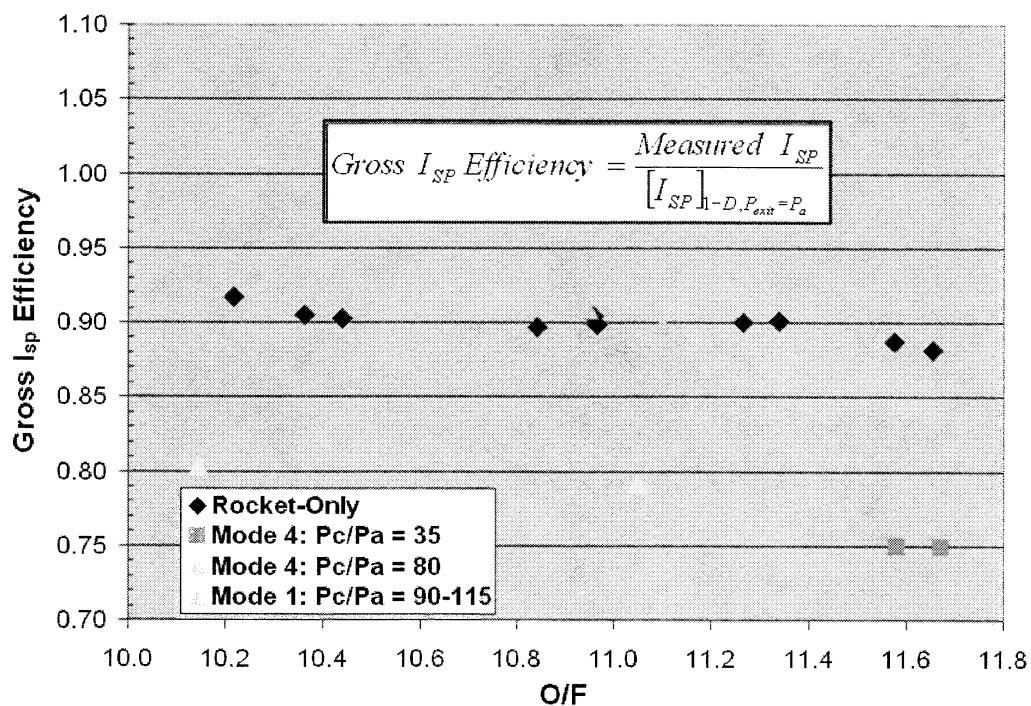
Figure 18. Modes 1 and 4 Summary Performance Data

21
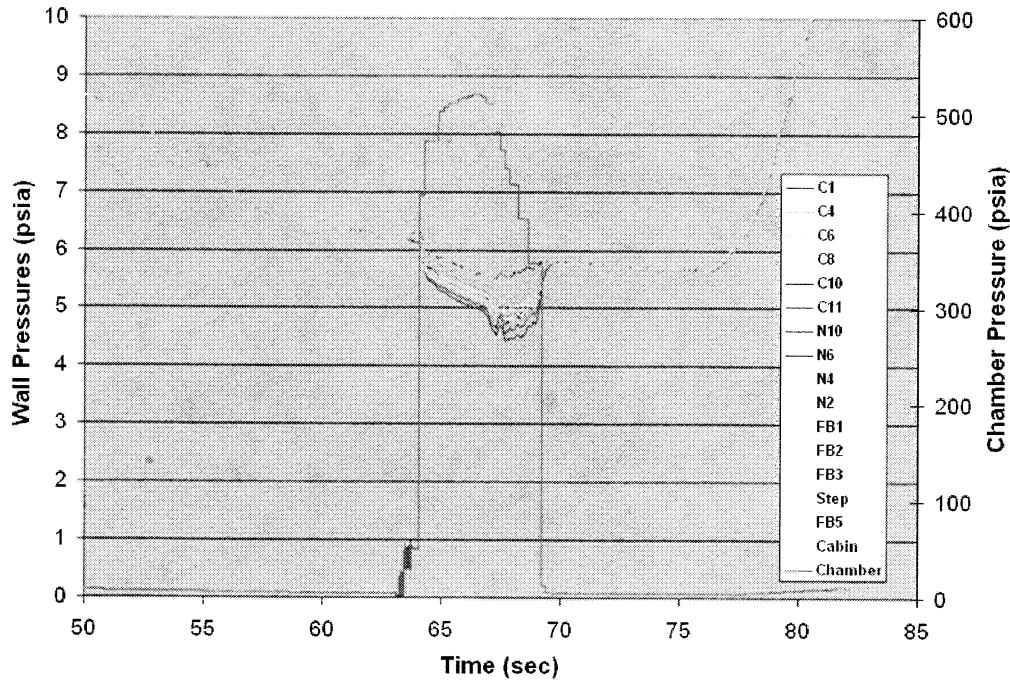
Figure 19. Wall Pressure Data for a nominal Mode 1 Test
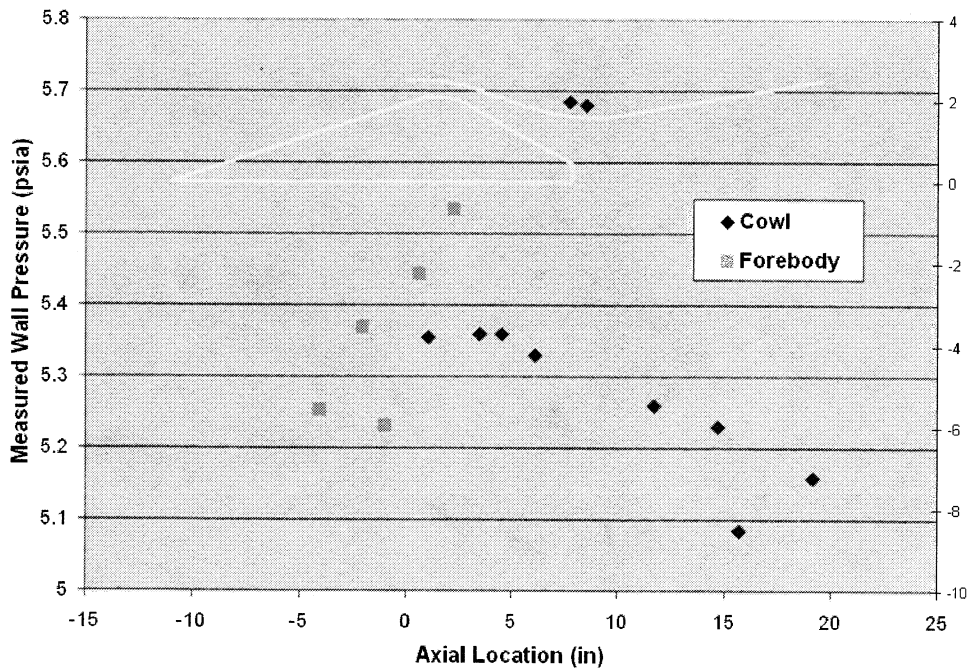
Figure 20. Time Averaged Wall Pressures During Rocket On Condition (Mode 1)
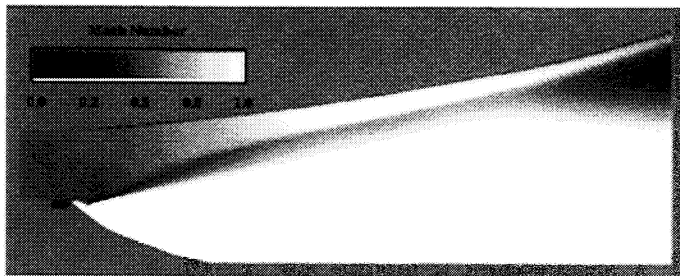
Figure 21. Mode 1 CFD results for IRS Cycle [Reference 4]
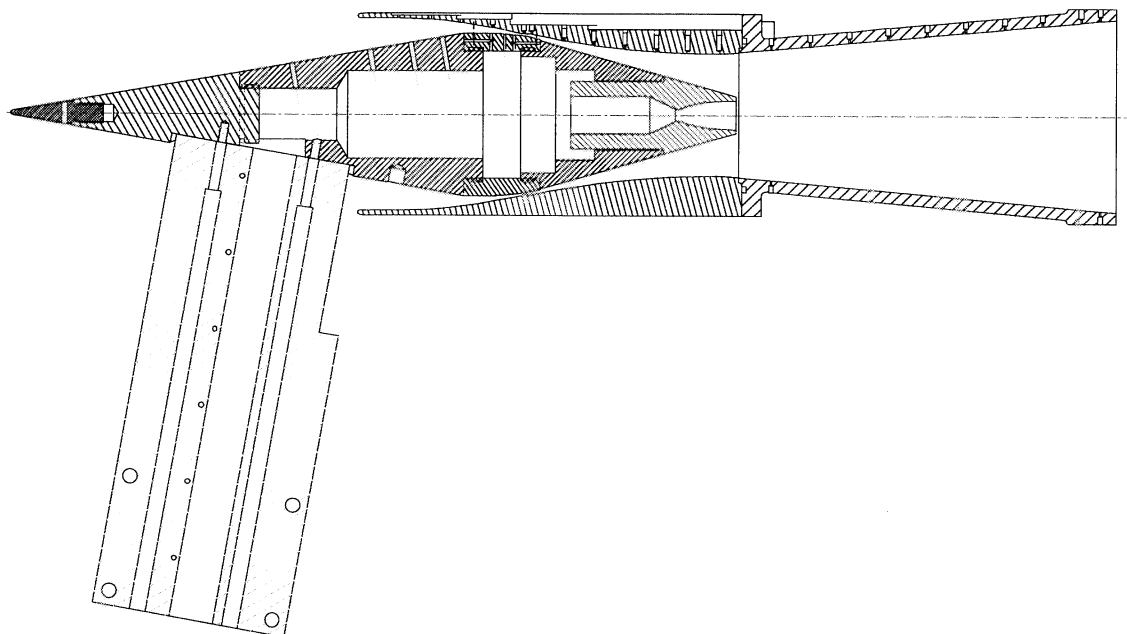
Figure 22. Mode 4 Engine Configuration
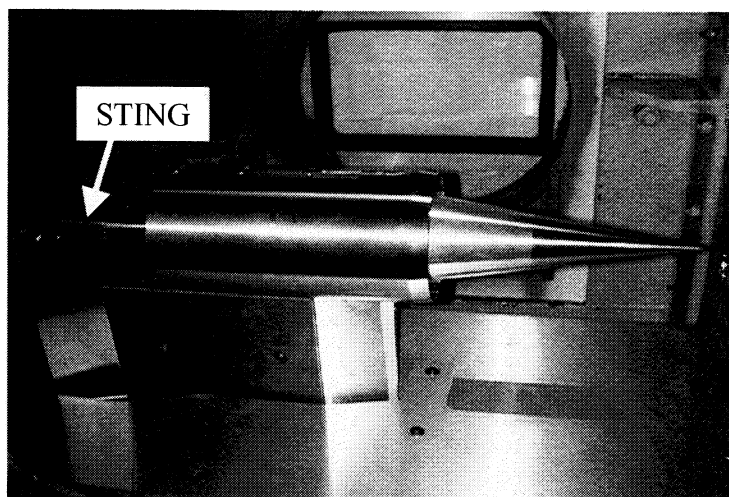
Figure 23. Mach 4 Inlet Model Installation in Cell 2

23
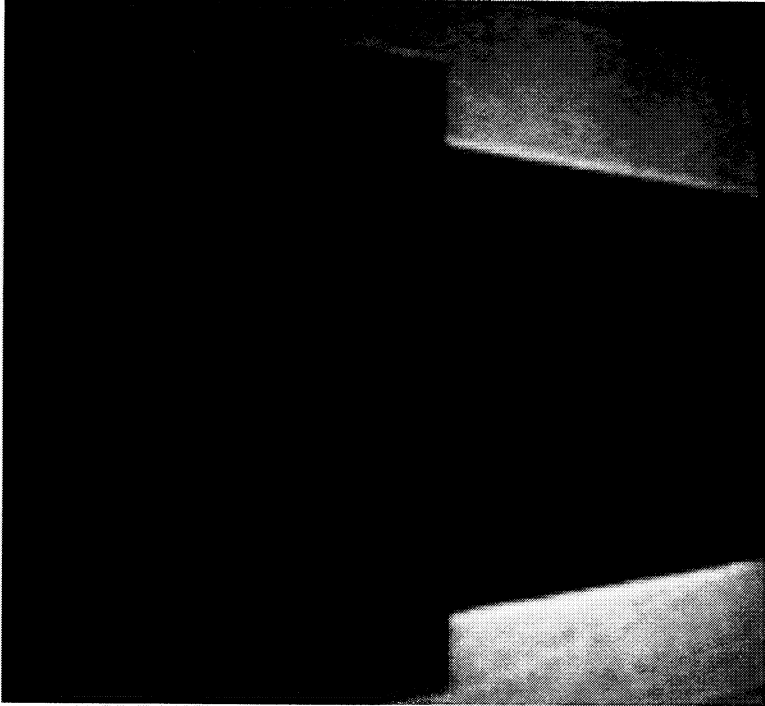
Figure 24. Flowfield During Forebody Translation (Inlet Started)
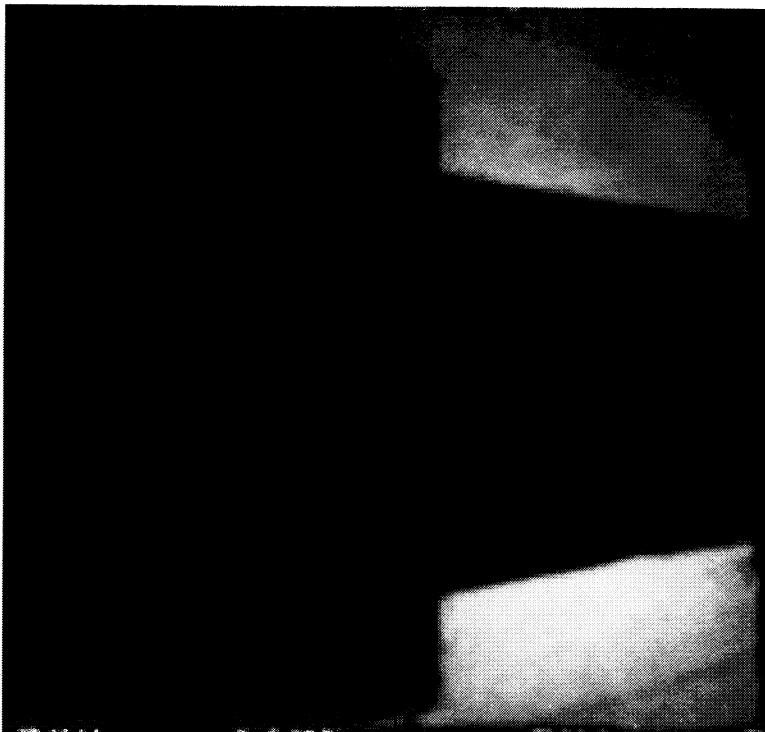
Figure 25. Flowfield During Inlet Unstart
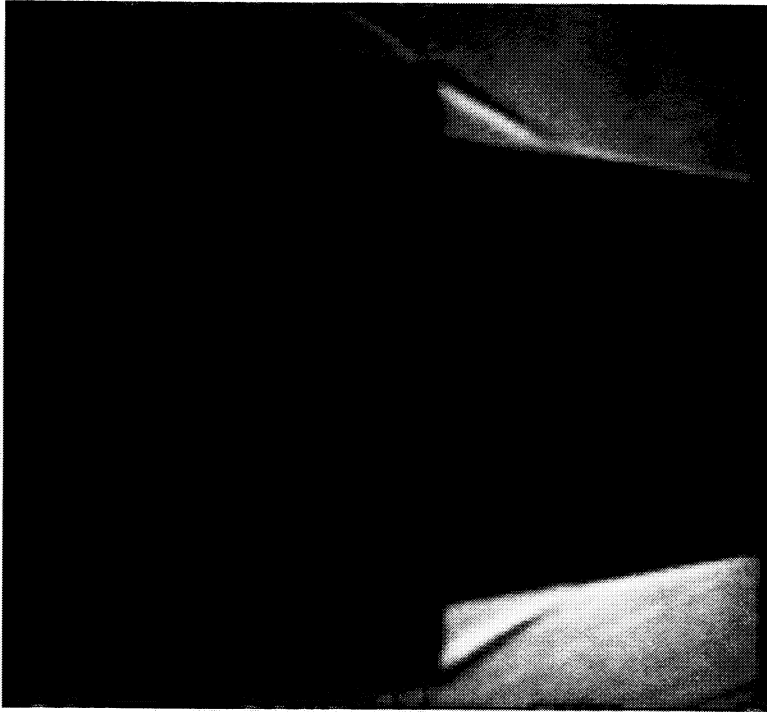
Figure 26. Flowfield Just Before Inlet Restart
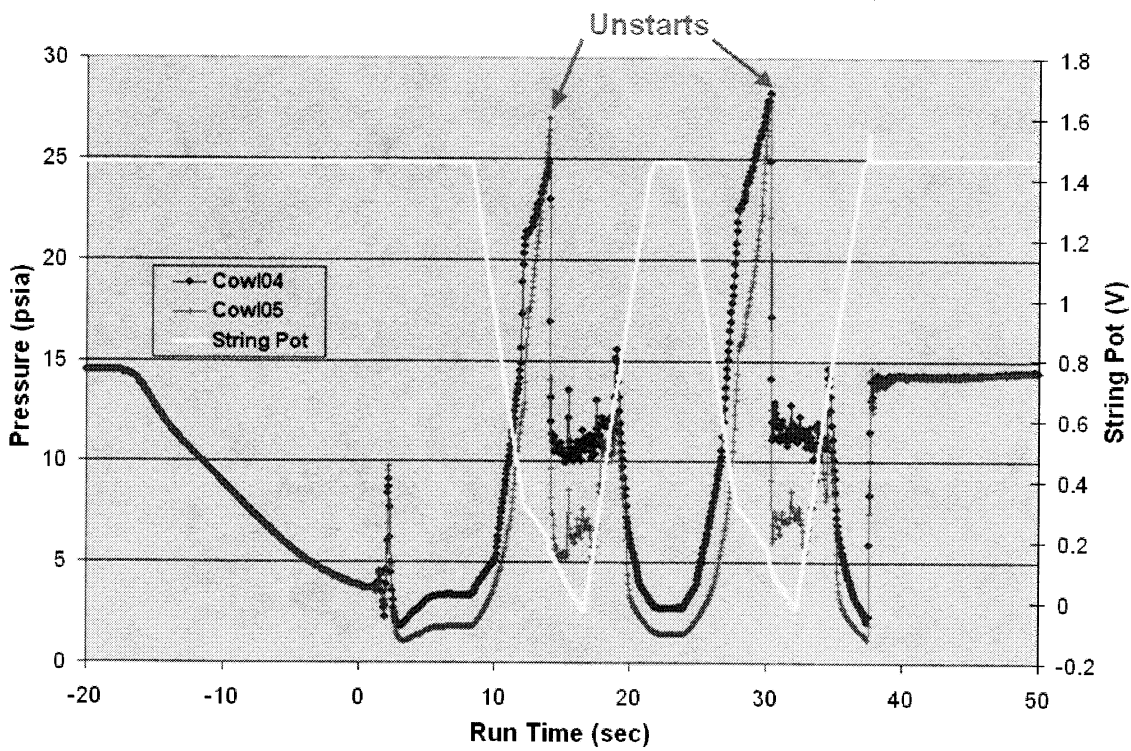
Figure 27. Inlet Test Data Showing Unstart
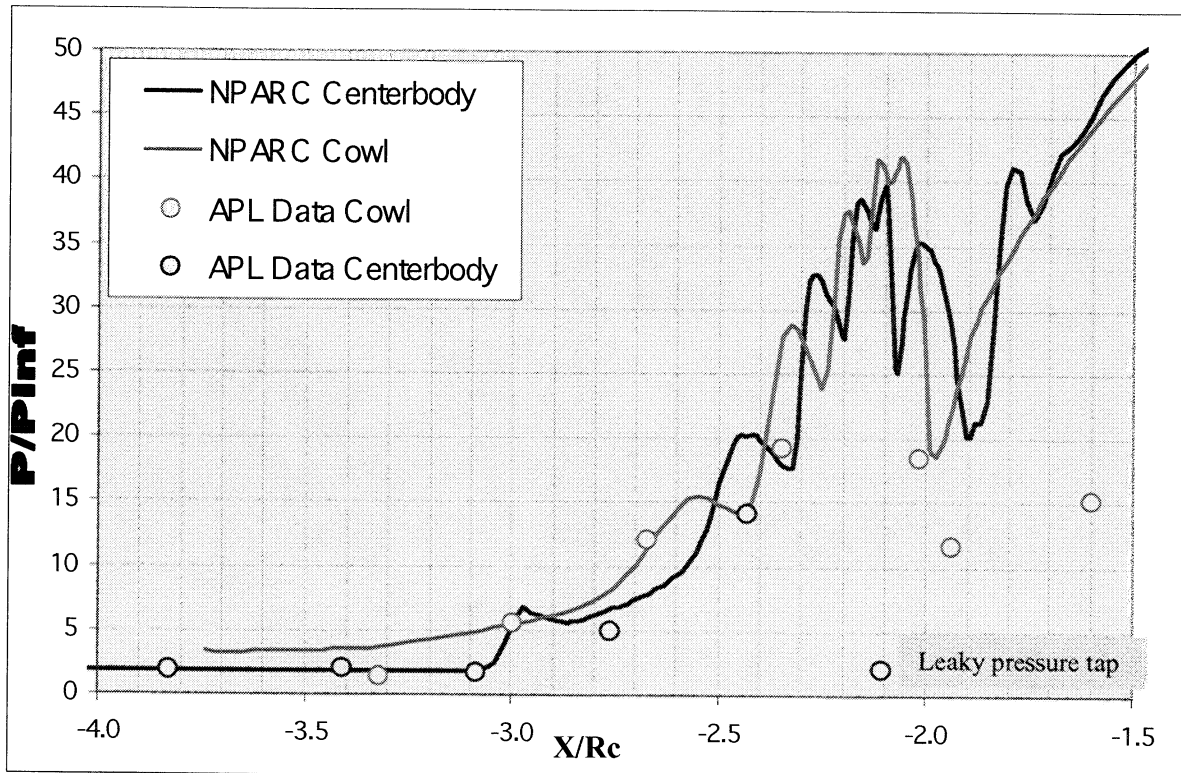
Figure 28. CFD and Experimental Results Comparison

Appendix A
Performance Analysis Summary

The following description will provide the step-by-step procedures used in determining the engine performance parameters for the rocket-only, Mode 1 and Mode 4 tests.

For all testing, facility, rocket chamber pressure and gross thrust measurements were taken. An example of this data, taken from test T106, is shown in Figure A1. This test data will be used to describe the entire performance methodology unless otherwise noted. A listing of the parameter names and their corresponding meanings are presented in Table A1.
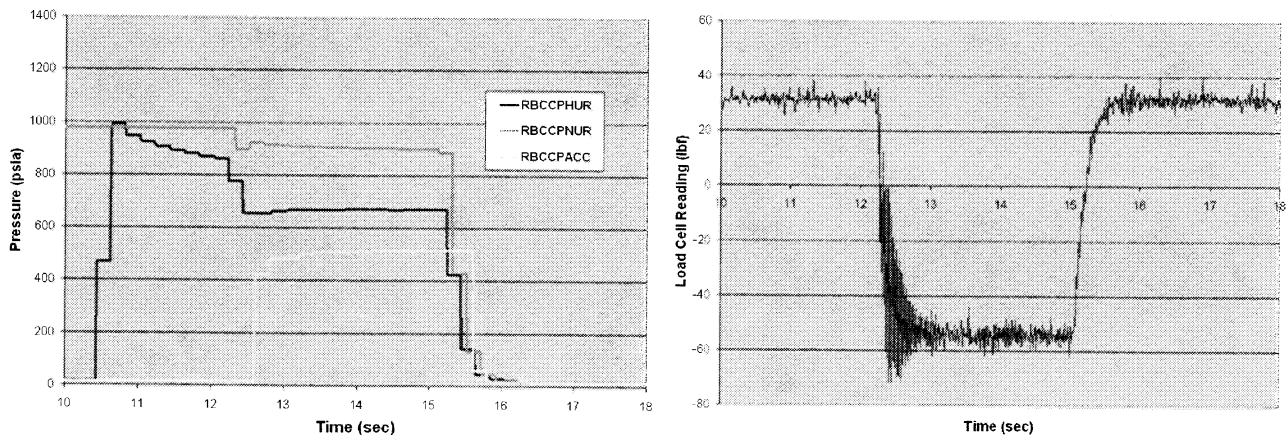
Figure A1. T106 Test Data

Based on the venturi supply pressures (RBCCPHUR and RBCCPNUR) and the rocket chamber pressure (RBCCPACC), a steady-state portion of the test (time = 13.4–15.1 seconds) was determined. Engine performance was then determined for each time step within this steady state portion. The data measurements recorded for a portion of the steady-state period is shown below.

| T106 Time	BARO	RBCCLoadCell	RBCCLoadExc	RBCCTADM1	RBCCTNitrox	RBCCTH2	RBCCPHDR	RBCCPHUR	RBCCPNDR	RBCCPNUR	RBCCPACC	Load Cell
sec	Psia	VDC	VDC	Deg F	Deg F	Deg F	psia	psia	psia	psia	psia	LBF
13.40	14.499	-0.000701	5.9797	68.66	46.60	64.97	635.32	668.24	791.79	909.39	502.17	-52.04
13.41	14.499	-0.000823	5.9806	68.45	46.39	64.72	635.32	668.27	792.40	909.39	505.24	-57.25
13.42	14.499	-0.000792	5.9796	68.59	46.47	64.72	635.20	668.20	792.40	909.31	505.28	-55.92
13.43	14.499	-0.000747	5.9799	68.53	46.26	64.70	635.75	668.24	792.40	909.39	505.28	-54.00
13.44	14.499	-0.000731	5.9803	68.59	46.53	64.61	635.38	670.07	792.32	909.31	505.24	-53.32
13.45	14.499	-0.000624	5.9799	68.52	46.26	64.66	635.63	670.10	792.40	909.31	505.28	-48.76
13.46	14.499	-0.000762	5.9796	68.45	46.25	64.90	635.08	670.07	792.40	909.39	505.24	-54.64
13.47	14.499	-0.000853	5.9803	68.46	46.12	64.61	636.24	670.03	792.32	909.39	505.24	-58.53
13.48	14.499	-0.000701	5.9799	68.52	46.05	64.45	635.44	670.07	792.40	909.39	505.24	-52.04
13.49	14.499	-0.000747	5.9806	68.53	46.12	64.71	636.36	670.10	792.48	909.39	505.28	-54.01
13.50	14.499	-0.000762	5.9805	68.45	46.05	64.83	635.99	670.07	792.32	909.39	505.24	-54.65
13.51	14.499	-0.000762	5.9791	68.52	45.91	64.31	635.63	670.07	792.40	909.39	505.28	-54.64
13.52	14.499	-0.000731	5.9797	68.53	45.85	64.51	635.50	670.03	792.40	907.63	505.28	-53.32
13.53	14.499	-0.000762	5.9787	68.59	45.98	64.59	636.36	670.07	792.48	907.56	505.24	-54.64
13.54	14.499	-0.000777	5.9806	68.59	46.05	64.48	635.69	670.07	792.32	907.48	505.28	-55.29
13.55	14.499	-0.000518	5.9791	68.45	45.71	64.38	636.30	669.99	792.32	907.56	505.28	-44.23
13.56	14.499	-0.000838	5.9802	68.59	45.98	64.51	636.48	670.03	792.40	907.48	505.28	-57.89
13.57	14.500	-0.000777	5.9793	68.51	45.62	64.55	636.18	670.03	792.40	907.56	505.24	-55.28
13.58	14.500	-0.000762	5.9788	68.52	45.43	64.26	636.24	670.07	792.32	907.56	505.24	-54.64
13.59	14.500	-0.000686	5.9791	68.52	45.77	64.70	637.09	670.10	792.32	907.56	505.28	-51.40
13.60	14.499	-0.000823	5.9803	68.51	45.49	64.29	636.97	670.03	792.40	907.56	505.47	-57.25
13.61	14.499	-0.000762	5.9800	68.59	45.36	64.49	636.30	670.03	792.40	907.56	507.53	-54.64

27

The load cell thrust measurement (LOAD CELL) is calculated based on an in-situ calibration performed before each test series or when the load cell was removed to be sent out for an annual calibration, and then replaced. For this data, the calibration was:

$$T = 42.897 * RBCCLoadCell * 1000 * \frac{RBCCLoadExc}{6.014} - 22.14$$

Fuel and oxidizer mass flows were then calculated using the sonic throat method for a real gas as described in the *Rocket-Only Testing* section of this report. A discharge coefficient of 1.0 was used for all cases. The results are shown below.

T106 Time	Oxidizer GAMMA	Mol Wt	R	M circle	P/Pt	P/Pt Mcircle	Venturi Diam	A Venturi	Mass Flow	Fuel GAMMA	Mol Wt	R	M circle	P/Pt	P/Pt Mcircle	Venturi Diam	A Venturi	Mass Flow
sec							in	in2	lbm/s							in	in2	lbm/s
13.40	1.520	30.006	51.4897	1.0940	0.5088	0.55670	0.1310	1.348E-02	0.2979	1.4	2.016	766.369	0.2656	0.5283	0.14030	0.0900	6.3617E-03	0.0260
13.41	1.520	30.006	51.4897	1.0940	0.5088	0.55670	0.1310	1.348E-02	0.2980	1.4	2.016	766.369	0.2656	0.5283	0.14030	0.0900	6.3617E-03	0.0260
13.42	1.520	30.006	51.4897	1.0940	0.5089	0.55670	0.1310	1.348E-02	0.2979	1.4	2.016	766.369	0.2656	0.5283	0.14030	0.0900	6.3617E-03	0.0260
13.43	1.520	30.006	51.4897	1.0940	0.5088	0.55670	0.1310	1.348E-02	0.2980	1.4	2.016	766.369	0.2656	0.5283	0.14030	0.0900	6.3617E-03	0.0260
13.44	1.520	30.006	51.4897	1.0940	0.5088	0.55670	0.1310	1.348E-02	0.2980	1.4	2.016	766.369	0.2656	0.5283	0.14030	0.0900	6.3617E-03	0.0261
13.45	1.520	30.006	51.4897	1.0940	0.5088	0.55670	0.1310	1.348E-02	0.2980	1.4	2.016	766.369	0.2656	0.5283	0.14030	0.0900	6.3617E-03	0.0261
13.46	1.520	30.006	51.4897	1.0940	0.5088	0.55670	0.1310	1.348E-02	0.2979	1.4	2.016	766.369	0.2656	0.5283	0.14030	0.0900	6.3617E-03	0.0261
13.47	1.520	30.006	51.4897	1.0940	0.5088	0.55670	0.1310	1.348E-02	0.2980	1.4	2.016	766.369	0.2656	0.5283	0.14030	0.0900	6.3617E-03	0.0261
13.48	1.520	30.006	51.4897	1.0940	0.5088	0.55670	0.1310	1.348E-02	0.2981	1.4	2.016	766.369	0.2656	0.5283	0.14030	0.0900	6.3617E-03	0.0261
13.49	1.520	30.006	51.4897	1.0940	0.5088	0.55670	0.1310	1.348E-02	0.2980	1.4	2.016	766.369	0.2656	0.5283	0.14030	0.0900	6.3617E-03	0.0261
13.50	1.520	30.006	51.4897	1.0940	0.5088	0.55670	0.1310	1.348E-02	0.2979	1.4	2.016	766.369	0.2656	0.5283	0.14030	0.0900	6.3617E-03	0.0261
13.51	1.520	30.006	51.4897	1.0940	0.5088	0.55670	0.1310	1.348E-02	0.2981	1.4	2.016	766.369	0.2656	0.5283	0.14030	0.0900	6.3617E-03	0.0261
13.52	1.520	30.006	51.4897	1.0939	0.5089	0.55667	0.1310	1.348E-02	0.2974	1.4	2.016	766.369	0.2656	0.5283	0.14030	0.0900	6.3617E-03	0.0261
13.53	1.520	30.006	51.4897	1.0939	0.5089	0.55667	0.1310	1.348E-02	0.2974	1.4	2.016	766.369	0.2656	0.5283	0.14030	0.0900	6.3617E-03	0.0261
13.54	1.520	30.006	51.4897	1.0939	0.5089	0.55667	0.1310	1.348E-02	0.2974	1.4	2.016	766.369	0.2656	0.5283	0.14030	0.0900	6.3617E-03	0.0261
13.55	1.520	30.006	51.4897	1.0939	0.5089	0.55667	0.1310	1.348E-02	0.2975	1.4	2.016	766.369	0.2656	0.5283	0.14030	0.0900	6.3617E-03	0.0261
13.56	1.520	30.006	51.4897	1.0939	0.5089	0.55667	0.1310	1.348E-02	0.2974	1.4	2.016	766.369	0.2656	0.5283	0.14030	0.0900	6.3617E-03	0.0261
13.57	1.520	30.006	51.4897	1.0939	0.5089	0.55667	0.1310	1.348E-02	0.2974	1.4	2.016	766.369	0.2656	0.5283	0.14030	0.0900	6.3617E-03	0.0261
13.58	1.520	30.006	51.4897	1.0939	0.5089	0.55667	0.1310	1.348E-02	0.2975	1.4	2.016	766.369	0.2656	0.5283	0.14030	0.0900	6.3617E-03	0.0261
13.59	1.520	30.006	51.4897	1.0939	0.5089	0.55667	0.1310	1.348E-02	0.2974	1.4	2.016	766.369	0.2656	0.5283	0.14030	0.0900	6.3617E-03	0.0261
13.60	1.520	30.006	51.4897	1.0939	0.5089	0.55667	0.1310	1.348E-02	0.2975	1.4	2.016	766.369	0.2656	0.5283	0.14030	0.0900	6.3617E-03	0.0261
13.61	1.520	30.006	51.4897	1.0939	0.5089	0.55667	0.1310	1.348E-02	0.2974	1.4	2.016	766.369	0.2656	0.5283	0.14030	0.0900	6.3617E-03	0.0261

Using the individual mass flow data, total mass flow and O/F ratio for each time step was determined. The characteristic exhaust velocity, C*, was also calculated for each time step (see Eq. 7). The results for these parameters are shown below.

Time	O/F	Mdot Total	C*
sec		lbm/s	ft/s
13.40	11.441	0.3239	6142.8
13.41	11.440	0.3240	6178.9
13.42	11.440	0.3240	6180.0
13.43	11.441	0.3240	6179.3
13.44	11.408	0.3241	6177.4
13.45	11.408	0.3241	6178.2
13.46	11.409	0.3240	6178.6
13.47	11.410	0.3241	6176.9
13.48	11.409	0.3242	6175.9
13.49	11.409	0.3241	6178.0
13.50	11.409	0.3241	6178.2
13.51	11.409	0.3242	6175.7
13.52	11.387	0.3236	6188.1
13.53	11.386	0.3235	6188.5
13.54	11.385	0.3235	6189.0
13.55	11.387	0.3236	6187.9
13.56	11.385	0.3235	6189.2
13.57	11.386	0.3235	6188.3
13.58	11.386	0.3236	6186.6
13.59	11.385	0.3235	6189.7
13.60	11.386	0.3236	6189.6
13.61	11.386	0.3235	6216.0

Gross thrust was determined by subtracting an average tare value from the load cell thrust data. In the example being presented, the tare value was the average load cell reading from time = 0–10 seconds. Vacuum thrust was then calculated using the following equation.

$$T_{vacuum} = T_{Gross} + P_{ambient}A_{exit}$$

Where $P_{ambient}$ is a measured valued (BAR0) for each time step. For the rocket-only tests, A_{exit} = 0.6691 in^2. For the Mode 1 and Mode 4 tests, A_{exit} = 19.635 in^2.

Specific Impulse (I_{sp}) and C* efficiencies were determined by dividing the experimental performance values by ideal, one-dimensional, performance values. These ideal values were determined in the following way. Average steady-state O/F ratio (11.340), chamber pressure (509.8 psia) and ambient pressure (14.50 psia) values were determined from the test data. Using these average values, the NASA GRC thermochemical equilibrium code, CEA, was used to determine ideal gross and vacuum I_{sp} values.

Ideal gross I_{sp} was determined be expanding the rocket flow to a pressure ratio equal to the measured chamber-to-ambient pressure ratio. Ideal vacuum I_{sp} was determined by expanding the rocket flow to the measured model area ratio with no back pressure. For all testing, pre- and post test measurements of the rocket throat diameter were taken to determine to correct area ratio. The exit diameter for the rocket-only tests was constant at 0.923 inches. The exit diameter for the Mode 1 and Mode 4 tests was constant at 5.0 inches. A nozzle efficiency of 1.0 was used al cases. The CEA code also outputs an ideal C* value. A summary of the CEA inputs and outputs used in this example is provided below.

Test Conditions	
Chamber Pressure (psia)	509.8
O/F Ratio	11.340
Ambient Pressure (psia)	14.500
Rocket Throat Diameter (in)	0.396
Rocket Exit Diameter (in)	0.923
Calculated Inputs to CEA	
Engine Pressure Ratio	35.16
Nozzle Area Ratio	5.433
CEA Results	
C* (ft/s)	6300
Vacuum Isp (lbf-sec/lbm)	324.88
Gross Isp (lbf-sec/lbm)	294.62

It should be noted again that during the Mode 1 and Mode 4 testing, the engine nozzle was likely separated, resulting in vacuum performance numbers that are meaningless using this method. The data below shows the time-wise calculation of the performance values. Average values of these results are considered as the overall engine performance and are presented in Table 2 of this report.

T106

Time sec	ETA C*	Gross Thrust	Gross Isp	ETA Gross Isp	Vacuum Thrust	Isp Vac	ETA Isp Vac
13.40	0.975	83.38	257.4	0.874	93.08	287.3	0.884
13.41	0.981	88.59	273.4	0.928	98.29	303.3	0.934
13.42	0.981	87.26	269.3	0.914	96.96	299.3	0.921
13.43	0.981	85.34	263.4	0.894	95.04	293.3	0.903
13.44	0.981	84.66	261.2	0.887	94.36	291.1	0.896
13.45	0.981	80.09	247.1	0.839	89.79	277.1	0.853
13.46	0.981	85.98	265.3	0.901	95.68	295.3	0.909
13.47	0.980	89.86	277.3	0.941	99.56	307.2	0.946
13.48	0.980	83.38	257.2	0.873	93.08	287.1	0.884
13.49	0.981	85.34	263.3	0.894	95.04	293.3	0.903
13.50	0.981	85.98	265.3	0.901	95.68	295.3	0.909
13.51	0.980	85.97	265.2	0.900	95.68	295.1	0.908
13.52	0.982	84.66	261.6	0.888	94.36	291.6	0.898
13.53	0.982	85.97	265.7	0.902	95.67	295.7	0.910
13.54	0.982	86.62	267.8	0.909	96.32	297.7	0.916
13.55	0.982	75.57	233.5	0.793	85.27	263.5	0.811
13.56	0.982	89.22	275.8	0.936	98.92	305.8	0.941
13.57	0.982	86.62	267.7	0.909	96.32	297.7	0.916
13.58	0.982	85.97	265.7	0.902	95.67	295.6	0.910
13.59	0.982	82.73	255.8	0.868	92.44	285.8	0.880
13.60	0.982	88.58	273.7	0.929	98.29	303.7	0.935
13.61	0.987	85.98	265.7	0.902	95.68	295.7	0.910

Table A1. Performance Analysis

Parameter	Units	Explanation
Time	sec	Run time
BARO	Psia	Barometric Pressure
RBCCLoadCell	VDC	Load Cell Output
RBCCLoadExc	VDC	Load Cell Excitation Voltage
RBCCTADM1	Deg F	Ambient Temperature
RBCCTNitrox	Deg F	Oxidizer Supply Temperature
RBCCTH2	Deg F	Fuel Supply Temperature
RBCCPHDR	psia	Pressure Downstream of Fuel Venturi
RBCCPHUR	psia	Fuel Supply Pressure (Upstream of Venturi)
RBCCPNDR	psia	Pressure Downstream of Oxidizer Venturi
RBCCPNUR	psia	Oxidizer Supply Pressure (Upstream of Venturi)
RBCCPACC	psia	Rocket Chamber Pressure
Load Cell	LBF	Load Cell Thrust Reading
GAMMA		Ratio of specific heats
Mol Wt		Molecular Weight
R	ft-lbf/(lbm-R)	Gas Constant
M circle		Eq. 3
P/Pt		Ratio of Static-to-Total Pressure
P/Pt Mcircle		Multiplication of the Above 2 terms
Venturi Diam	in	Flow Venturi Diameter
A Venturi	in2	Flow Venturi Area
Mass Flow	lbm/s	Mass Flow
O/F		Oxidizer/Fuel Ratio
C*	ft/s	Characteristic Exhaust Velocity (Eq. 7)
ETA C*		C* Efficiency
Gross Thrust	lbf	Engine Gross Thrust (Eq. 4)
Gross Isp	sec	Engine Gross Specific Impulse (Eq 4)
ETA Gross Isp		Gross Specific Impulse Efficiency (Eq. 6)
Vacuum Thrust	lbf	Engine Vacuum Thrust
Isp Vac	sec	Engine Vacuum Specific Impulse
ETA Isp Vac		Vacuum Specific Impulse Efficiency